Int. J. Electrochem. Sci., 15 **(2020)** 5758 – 5769, doi: 10.20964/2020.06.55

International Journal of
ELECTROCHEMICAL
SCIENCE
www.electrochemsci.org

Improving the Properties of Nickel Organic Framework as Electrode Materials for supercapactiors by Introducing Functional Groups

Ben Lei, Cailing Wu, Mei Li, Lifang Jia, Guoping Wang[*]

College of Chemical Engineering, University of South China, Hengyang 421001, China
[*]E-mail: wgpcd@aliyun.com

Received: 29 January 2020 / *Accepted:* 25 March 2020 / *Published:* 10 May 2020

To improve the redox activity of metal organic framework (MOF), functional groups have been introduced into organic framework to prepare Ni–MOF–NO_2 and Ni–MOF–NH_2 with solvothermal method. Physical and electrochemical characterization using SEM, EDS, XRD and BET shows that Ni–MOF–NH_2 possesses thinner sheet–like structure, higher specific surface area and excellent electron transfer ability, which have activated the metal center Ni. A specific capacitance as high as 1024.4 F g^{-1} has been achieved for Ni–MOF–NH_2 in the potential window of 0–0.45 V at 100 mV S^{-1}, much higher than that of Ni–MOF–NO_2 (353.9 F g^{-1}) and Ni–MOF (399.5 F g^{-1}). The introduction of electron–donating group –NH_2 not only influences the morphology and specific surface area of MOF material, but also increases the electron cloud density of the metal active center, activates metal center Ni and alleviates the polarization of electrode.

Keywords: Metal organic framework; supercapacitor; Functional Group

1. INTRODUCTION

Metal organic framework (MOF) compounds can be characterized as superior porous structure, adjustable pore size, low density and large specific surface area.[1,2] Especially, by means of tailoring metal center and organic ligand, they can be easily modulated to acquire the desired properties involving topology, pore structure, active metal center, chemical functionality and electron conductivity. Such a property tunability has attracted increasing attention, and researchers are attempting to investigate MOF for numerous potential practice applications including gas storage, drug delivery and imaging, catalysis, chemical separation, sensor and energy conservation etc. [1][3-5]

As a promising energy storage device, supercapacitor can be extensively used in transportation, energy conservation and uninterruptible power sources etc. Its widespread applications are mainly based

on the characteristics—high power density, long cycle life and high efficiency, which are significantly affected by the electrode materials. Therefore, it is necessary to carefully design and tune electrode materials. People are sparing no efforts to develop new electrode materials. As suggested by Conway, [6] the electrode materials for supercapacitor generally require high specific areas, excellent intra-/inter-particle conductivity and better electrolyte accessibility. MOF's large specific surface area, superior porous structure and accessible metal sites make it very suitable for supercapacitor electrode material. The large specific surface area facilitates the storage of electrical double-layer capacitance, and the porous structure extending in all directions is helpful for ion transportation. Moreover, active metal can provide the fast and reversible redox reactions, giving rise to faradic capacitance. For example, using ultrasonication process, Yan has prepared accordion-like MOF with a capacitance of 988 F g^{-1} at 1.4 A g^{-1} [7] and Yang has synthesized (2D)Ni–MOF exhibiting a capacitance of 1127 F g^{-1} at a current density of 0.5 A g^{-1}. [8] Here, it is necessary to point out that the above excellent properties of MOF are often accompanied by the decrease in redox activity. In fact, the redox processes can dramatically increase the specific capacitance of supercapacitors by 10–100 times and extend the working voltage simultaneously. [9] Therefore, to popularize MOF as supercapacitor electrode material, it is very important to improve the redox activity of MOF. As reported in the reference, [10] the variation of electron state within MOF can change its electron transfer ability and then electrochemical activity. Here, we attempt to decorate MOF with functional group to present charge distributions complementary to organic framework or metal center for addressing the redox activity of MOF. With respect to the metal center, because nickel-based materials have the properties involving thermal and chemical stability, high theoretical specific capacitance, low-cost and environmental benignity, [11] nickel has been selected to serve as the metal center.

2. EXPERIMENTAL

2.1 Materials synthesis

All chemicals were reagent grade and used without further purification. To prepare Ni–MOF, $Ni(NO_3)_2 \cdot 6H_2O$ (1 mmol) and terephthalic acid (1 mmol) were dispersed in dimethyl formamide (20 ml) and stirred for 40 min. Then, NaOH (0.2 mol) was added and additional continuous stirring lasted for 20 min. The above homogeneous solution was then transferred to a Teflon–lined stainless–steel autoclave and kept for 15 h at 100 ℃. After cooled down to room temperature, the obtained products were washed with ethanol and then dried at 50 ºC for 8 h. For a comparative study, electron–withdrawing and electron–donating groups were introduced into organic framework to prepare Ni–MOF–NO_2 and Ni–MOF–NH_2. The preparing process was completely similar to that of Ni–MOF except that the raw material terephthalic acid was replaced with 2–nitroterephthalic acid and 2–aminoterephthalic acid, respectively.

2.2 Physical Characterization of materials

The morphology and structure of the three samples were identified with field–emission scanning electron microscopy (FESEM, Hitachi SU-8010). Prior to examination, a thin layer of gold was sputtered on the samples' surface. Nitrogen adsorption−desorption measurements were performed with an 3H–2000 series analytical instruments using N_2 as an adsorptive agent at 77.3 K. The specific surface area and the pore–size distribution were determined by Brunauer–Emmett–Teller (BET) and Barrett–Joyner–Halenda (BJH) analyses. Scanning transmission electron microscopy (STEM) JEOL JEM-ARM200F TEM/STEM, which was operated at 200 kV, was used for obtaining the energy dispersive X-ray spectroscopy (EDS) mapping images. Elemental distribution of materials was determined by X-ray photoelectron spectroscopy (XPS), and the functional groups in three materials were explored by Fourier transform infrared spectrometer (FTIR) .

2.3 Electrochemical measurements

The electrochemical performance of the above MOF material was investigated using a three–electrode cell configuration in a 4 M KOH aqueous electrolyte. Platinum foil and a saturated calomel electrode were utilized as the counter and reference electrodes, respectively. Glassy carbon coated by the prepared MOF materials served as the working electrode.

The working electrodes was prepared as the following procedure. Firstly, carbon nanotubes (1.5 mg) and MOFs (7.5 mg) were dispersed under ultrasonication for 30 min in 5.0 ml isopropanpol to form homogeneous solution. Then, 5.0 μl of the above solution was pipetted gradually onto the surface of glassy carbon electrode. After naturally drying, 5 μl of the dilated Nafion® solution (0.1% wt%, Aldrich) was covered on the surface of glass carbon electrode to form an electrode protection layer. The samples' electrochemical performances were characterized by cyclic voltammograms (CV) within a potential window ranging from 0 to 0.45 V (vs. SCE) at 100 mV S^{-1} potential scanning rate. The chronopotentiometry window voltage ranging from 0-0.35 V. The EIS was measured within a frequency range of 0.1~100000 Hz.

3. RESULTS AND DISCUSSION

The morphology of these materials were characterized by field–emission scanning electron microscope (FESEM). As shown in Fig. 1, Ni–MOF–NH_2 displays a thinner sheet–like structure, and these sheets help to form numerous mesopores. Although Ni–MOF and Ni–MOF–NO_2 also consist of sheets, these sheets are much thicker than that of Ni–MOF–NH_2 and they stack to form thicker laminates. As the result, they may show some lower specific surface area than Ni–MOF–NH_2.

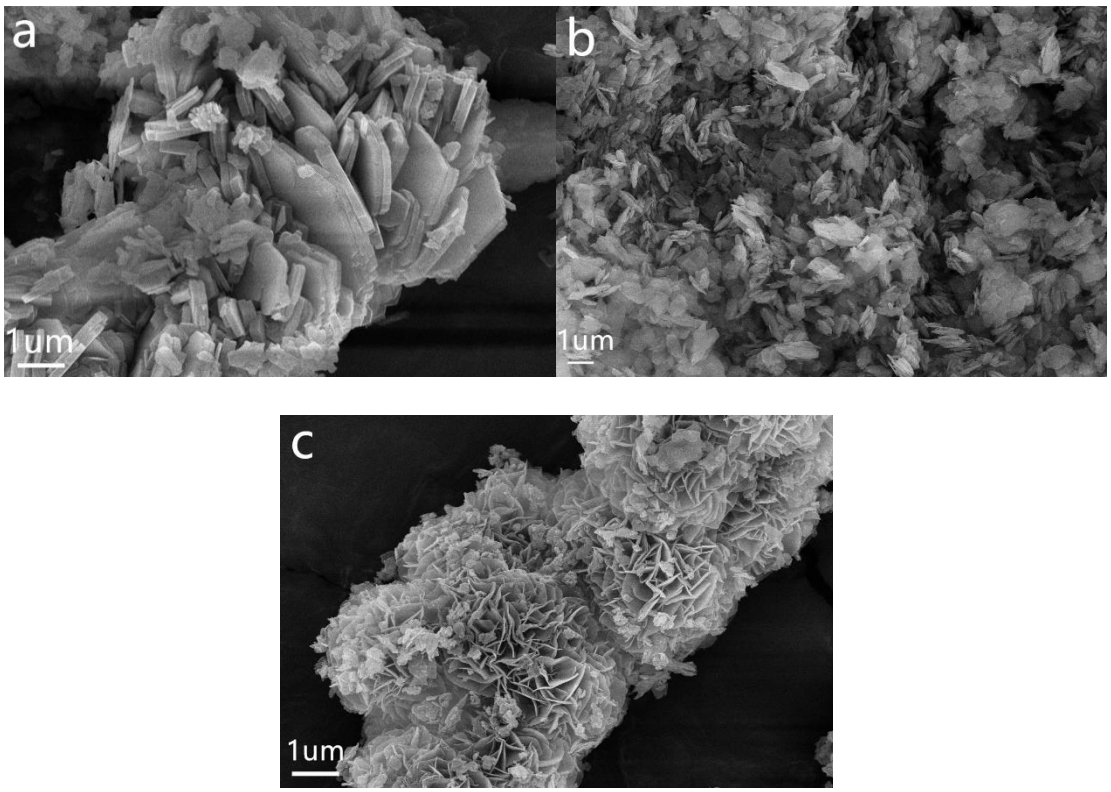

Figure 1. SEM images of (a) Ni–MOF–NO_2, (b) Ni–MOF and (c) Ni–MOF–NH_2

As shown in Fig. 2(a), the adsorption/desorption isotherms of Ni–MOF and Ni–MOF–NO_2 almost overlap on each other, implying that their pore distributions are some similar. Nevertheless, Ni-MOF-NH_2 shows some difference. When increasing the partial pressure to the range of 0.4–0.7, Ni-MOF-NH_2 exhibits an obvious H3-type hysteresis loop. Such a hysteresis points to the presence of mesopores. This is further confirmed by pore-size distribution curves.

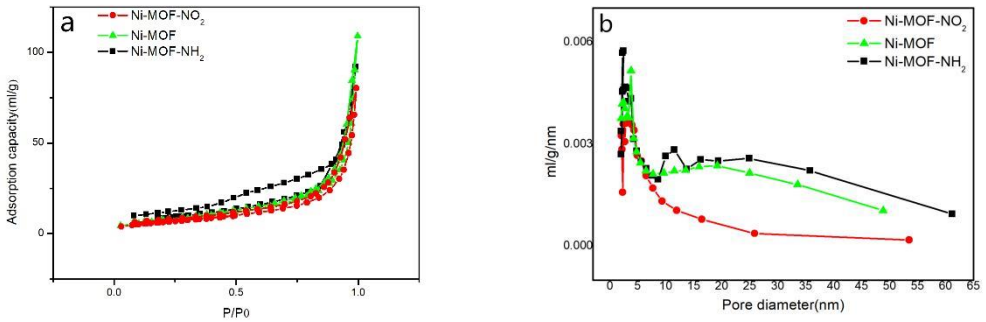

Figure 2. (a) N_2 adsorption/desorption isotherms; (b) the pore-size distribution

As shown in Fig. 2(b), Ni-MOF-NH_2 displays apparently larger number of mesopores, and the corresponding differential pore volume of Ni–MOF–NO_2 and Ni–MOF and Ni-MOF-NH_2 is 0.1071, 0.1783 and 0.1556 ml g^{-1}, and their obtained specific surface area is 21.8, 27.3 and 34.2 m^2 g^{-1}, respectively. The higher specific surface area of Ni–MOF–NH_2 may be attributed to its thinner sheets

and a large amount of mesopores as observed in SEM. Appropriate mesopores may be necessary for connecting micropores, increasing the specific surface area.

From the STEM-EDS mapping of Ni-MOF-NH_2 (Fig. 3), the highly uniform distribution of the elements Ni, O and N can be observed, indicating Ni and the ligand 2–aminoterephthalic acid are homogeneously incorporated into Ni-MOF-NH_2. The elementary composition of the three samples are further confirmed by X-ray photoelectron spectroscopy (XPS). The contents of Ni in Ni-MOF-NO_2 and Ni–MOF and Ni-MOF-NH_2 are 1.76%, 2.09% and 1.96%, respectively.

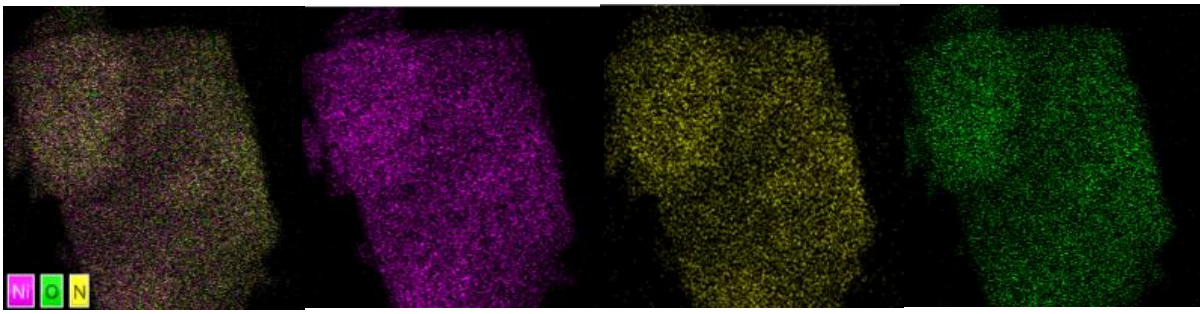

Figure 3. STEM-EDS mapping of Ni-MOF-NH_2

The detailed structure information of Ni–MOF–NO_2, Ni–MOF and Ni–MOF–NH_2 was further identified by fourier transform infrared spectrometer (FTIR) and X-ray diffraction (XRD).

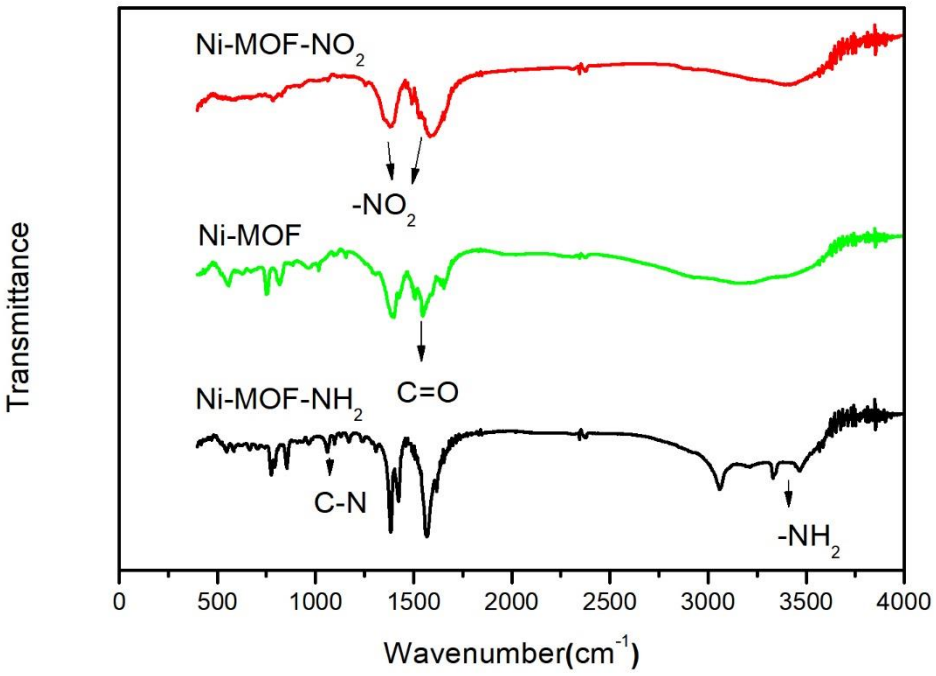

Figure 4. FTIR spectra of Ni-MOF-NO_2, Ni-MOF and Ni-MOF-NH_2

As shown in Fig. 4, in the range of 1350-1650 cm^{-1}, the IR absorption patterns of Ni ion coordinated –COO moiety are some similar in all the three MOF materials. [12] It should be pointed out that the peaks of Ni–MOF–NO_2 obviously become broader. This phenomenon is because that –NO_2 and –COO resonate at a close frequence. The peaks locating at 1597.8 cm^{-1} and 1404 cm^{-1}, which are attributed to the character peaks of –NO_2 and result from the shift of V^{as}_{NO2}, $V^{s}_{NO2,}$ overlap with the character peaks of –COO to some extent, resulting in a broader peaks in Ni–MOF–NO_2. In addition, Ni–MOF–NH_2 exhibits characteristic double peaks of the group –NH_2 at about 3380 and 3500 cm^{-1}.

The XRD analysis showed the crystal structure and crystallinity, and the sharp peaks showed good crystallinity. As shown in Fig. 5, Ni-MOF and Ni-MOF-NH_2 have sharp peaks and their crystallinity is much better than that of Ni-MOF-NO_2. After introducing the functional group -NH_2, the crystal structure of Ni-MOF has changed. The peaks locating at 2θ=7.5, 11.0, 12.4, 13.4, 19.8, and 25.8° in Ni-MOF disappeared in Ni-MOF-NH_2, and some new peaks appeared at 2θ=14.5, 16.7, and 29.7°.

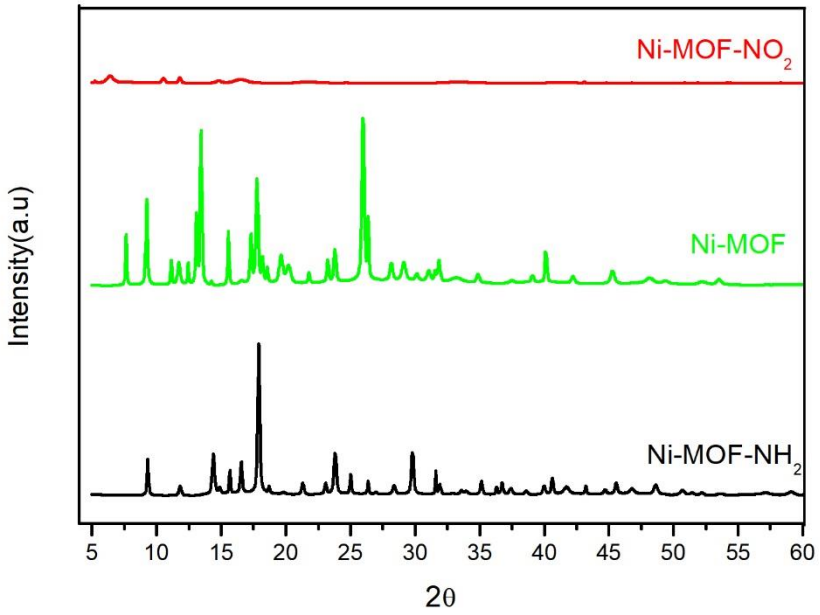

Figure 5. XRD patterns of Ni-MOF-NO2 , Ni-MOF and Ni-MOF-NH_2

According to valence band spectra provided by Fig. 6, introducing functional groups into MOF has obviously changed the binding energy of metal Ni 2p 3/2, suggesting the modulation of electronic structure in MOF materials[10]. Compared with that of Ni–MOF, the binding energy of Ni 2p 3/2 in Ni–MOF–NO_2 shifts to a higher energy. The shift value is 0.8 eV. Since the functional group –NO_2 belongs to electron–withdrawing group, it can make electrons closer to itself and far away from other elements such as metal. This in turn decreases the electron cloud density around metal Ni. On the contrary, for Ni–MOF–NH_2, a red shift value of 1.5 eV can be observed relative to Ni–MOF. Because the functional group –NH_2 is an electron–donating group, it can provide more electrons to the metal center, resulting in an increase in the electron cloud density of the metal active center.

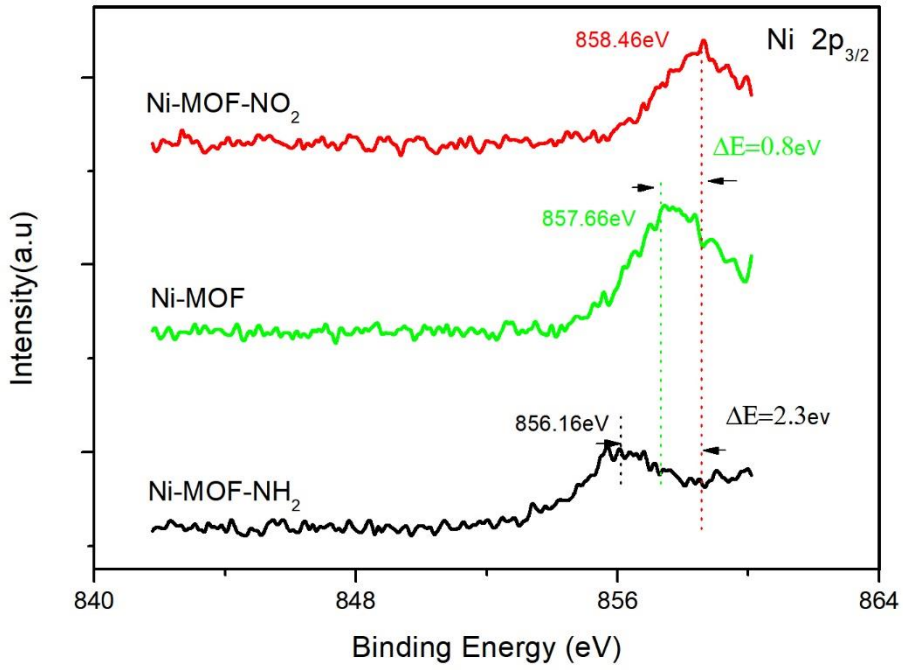

Figure 6. Ni 2p 3/2 spectra of Ni–MOF–NO_2, Ni–MOF, Ni–MOF–NH_2

Fig. 7 (a) displays the CV curves of three MOF materials at a potential scan rate of 100 $mV.s^{-1}$. The surface anodic reaction peaks of Ni−MOF−NO_2, Ni−MOF and Ni−MOF−NH_2 are located near 0.37, 0.34, 0.29V, respectively. Their corresponding cathodic peaks are located near 0.221, 0.218, 0.175 V, respectively. Their average redox potentials are 0.296, 0.279,0.233 V, respectively. Compared with Ni−MOF, the anodic and cathodic peaks of Ni−MOF−NO_2 shift to a higher potential, while those peaks of Ni−MOF−NH_2 move to a lower potential. These phenomena imply that the electron−withdrawing group −NO_2 makes the redox of metal more difficult, and the electron−donating group −NH_2 makes the redox of metal easier. These phenomenon can be explained as the following. Electron−withdrawing group −NO_2 has pulled down the electron cloud density of metal Ni, making the electron transfer more difficult in Ni–MOF–NO_2 and passivating metal center Ni. Contrarily, electron–donating group –NH_2 completely acts in the opposite way, making the electron transfer much easier in Ni–MOF–NH_2 and activating metal center Ni. As the result, the specific capacitance of three MOF materials decreases in the order of Ni–MOF–NH_2, Ni–MOF and Ni–MOF–NO_2. The specific capacitance of Ni–MOF–NH_2 can reach 1024.4 F g^{-1}, while Ni–MOF–NO_2 only displays a specific capacitance of 353.9 F g^{-1}, which is even lower than that of Ni–MOF (399.5 F g^{-1}).

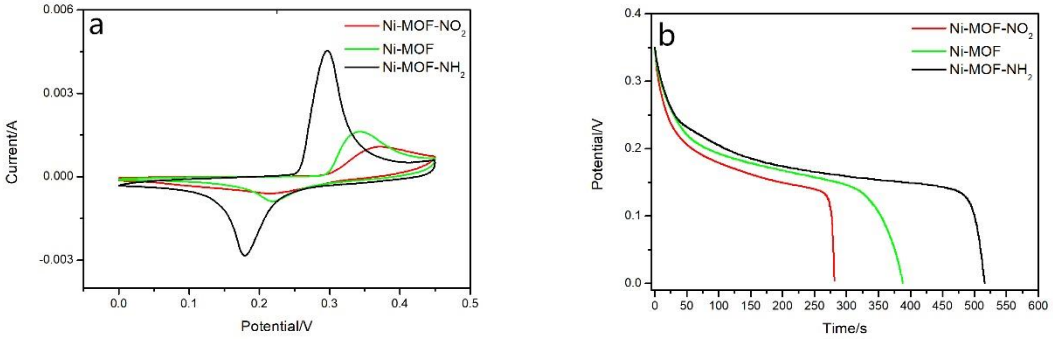

Figure 7. (a) CV of MOF at a potential scanning rate of 100 mv s^{-1}; (b) Galvanostatic discharging voltage profiles curves of MOF at the current density of 1 A g^{-1}

Their charge–discharge curves (Fig. 7(b)) show the similar trend. The plateaus between 0.13 and 0.3 V imply redox reactions for Ni, which are also observed in the CV curves (Fig. 7(a)). Obviously, among the the three MOF materials, Ni−MOF−NH_2 shows the longest plateau, and Ni−MOF−NO_2 displays the shortest one. The longer the plateau is, the higher the specific capacitance is. At the current density of 1 A g^{-1}, the calculated specific capacitances of Ni–MOF–NO_2, Ni–MOF and Ni–MOF–NH_2 are 750, 1010 and 1473 Fg^{-1}, respectively. As shown in Table 1, Ni–MOF–NH_2 shows much better performance than similar MOF materials reported in references. This comparision suggests that electron–donating group –NH_2 is helpful for improving the electrochemical activity of MOF.

Table 1. Comparison of Ni–MOF–NH_2 with references.

Material/substrate	Synthetic method	Electrolyte	Potential Window (V)	Current density (A g-1)	Cs (F g^{-1})	Ref.
Ni-MOF/AC	solvothermal	2 M KOH	0-0.5	1	804	[13]
Ni-MOF	solvothermal	1 M LiOH	0-0.5	0.5	306.8	[14]
Ni-MOF/AC	solvothermal	2 M KOH	0-0.48	1	781.2	[15]
Ni-MOF–NH_2	solvothermal	4 M KOH	0-0.45	1	1473	this work

In addition, we can learn something about the internal resistance and polarization from Fig. 7(b). According to the reference, [16] the relationship among discharge potential (Φ), open circuit potential (Φo), polarization potential (η) and internal resistance (R) can be written as the Equation (1).

$\Phi=\Phi_0 - (\eta + IR)$ (1)

When the discharging current I is fixed, the lower R will give rise to the lower IR and η, and then a higher Φ. In Fig.7(b) , Ni–MOF–NH_2 clearly exhibits the highest discharge potential plateau, and then followed by Ni–MOF and Ni–MOF–NO_2. This suggests that Ni–MOF–NH_2 exhibits the slightest polarization. This may be ascribed to its rapid electron transfer ability. The higher the electron density is, the easier the electron transfer becomes.[10] Because electron–donating group –NH_2 can donate

electrons and then increase the electron cloud density around metal Ni. As the result, the polarization is alleviated, and a higher and longer potential plateau is observed. Therefore, from electron transfer point, introducing electron–donating group is undoubtedly helpful for electron transfer in Ni–MOF electrode material, especially at higher potential scan rate.

As shown in Fig. 8, Ni–MOF–NH_2 displays higher specific capacity than Ni–MOF–NO_2 and Ni–MOF no matter what potential scan rate is. When the potential scan rate increases from 1 to 5 mV^{-1}, the specific capacitance of Ni–MOF–NO_2 and Ni–MOF decreases by about 300 F g^{-1}, much sharper than that of Ni–MOF–NH_2. The reasonable explanation is that Ni–MOF–NH_2 has the highest specific surface area, large amount of mesopores, higher electron transfer ability and higher active metal center.

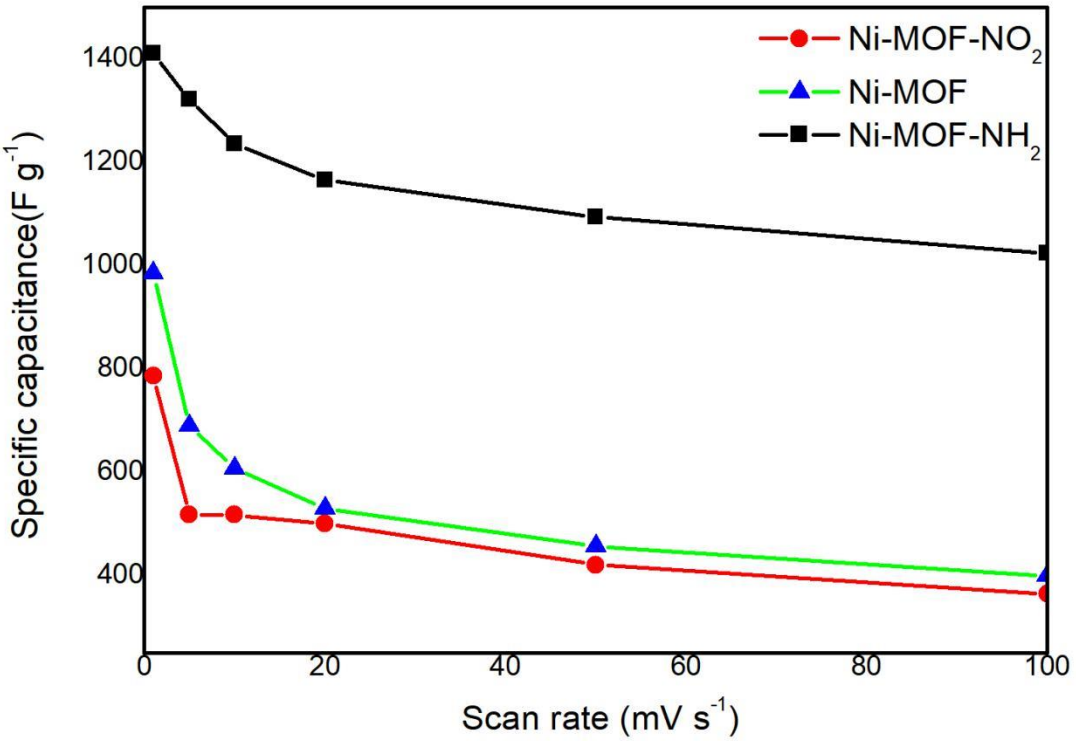

Figure 8. The initial specific capacitance Vs scan rate.

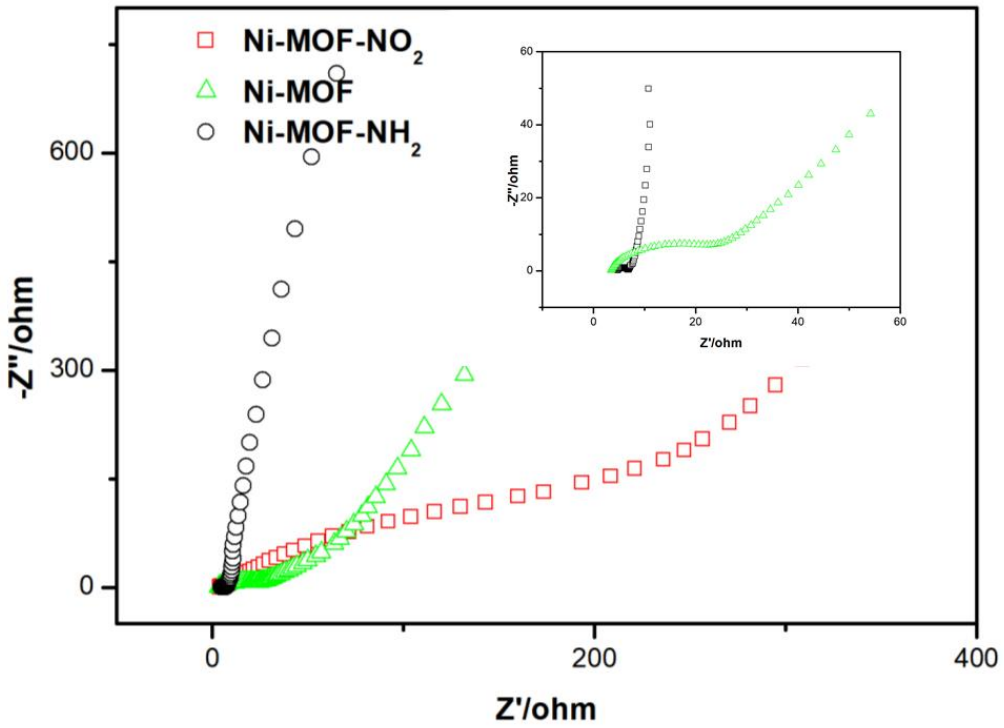

Figure 9. Impedance plots of Ni–MOF–NO_2, Ni–MOF and Ni–MOF–NH_2,

In the impedance plots, the semicircle in the high frequency region and the straight line in the low frequency region represent the charge transfer resistance and the diffusion rate of electrolyte ions, respectively. [17] Obviously, Ni–MOF–NH_2 shows much smaller semicircle and a straight line with a higher slope than Ni–MOF and Ni–MOF–NO_2 (Fig.9). This phenomenon implies Ni–MOF–NH_2 possesses lower electron resistance and lower ion diffusion resistance. Its lower electron resistance results from the introduction of group –NH_2. As described above, electron−donating group −NH_2 can increase the electron cloud density of metal Ni, making the electron transfer much easier. Meanwhile, Ni-MOF and Ni-MOF-NH_2's higher crystallinity may contribute to their higher electron conductivity. The lower ion diffusion resistance may be attributed to its thinner sheet. The thinner the sheet is, the shorter the diffusion distance of electrolyte ions, giving rise to a lower electrolyte diffusion resistance. In one word, the impedance plots have offered further evidence for the superior electrochemical performance of Ni–MOF–NH_2.

4. CONCLUSION

MOF often suffer from poor electrochemical activity, especially redox activity, limiting its specific capacitance. To improve its redox activity, functional groups –NH_2 and –NO_2 have been introduced into organic framework, respectively, and XRD, EDS and SEM were employed to characterize MOF material. Cyclic voltammetric methods were employed to study its redox process. The results showed that functional groups dramatically influence the structure and the properties of MOF.

Electron–donating group $–NH_2$ can result in a thinner sheet–like structure and higher specific surface area, while electron−withdrawing group $–NO_2$ leads to thicker laminates and a lower specific surface area. The thinner sheet shortens the diffusion distance of electrolyte ions, leading to a lower electrolyte diffusion resistance.

In addition, electron–donating group $–NH_2$ can increases the electron cloud density of the metal active center, activates metal center Ni, make the transfer of electron much easier and alleviates the polarization of electrode. Nevertheless, electron−withdrawing group $–NO_2$ has pulled down the electron cloud density of metal Ni and passivated metal center Ni, making the transfer of electron more difficult in Ni−MOF−NO_2.

Ni–MOF–NH_2 provides a specific capacitance of 1024.4 F g^{-1} in the potential window of 0–0.45 V at 100 mV S^{-1}, much higher than that of Ni–MOF–NO_2 (353.9 F g^{-1}) and Ni–MOF (399.5 F g^{-1}). Introducing electron–donating group is undoubtedly helpful for Ni–MOF electrode material, especially at higher potential scan rate.

ACKNOWLEDGMENTS

This work was supported by the Natural Science Foundation of Hunan Province, China (grant number 2019JJ60031), the Research Foundation of Education Bureau of Hunan Province, China (grant number 15B200), the Natural Science Foundation of Hunan Province, China (grant number 2016JJ3105) and the Postgraduate Science Foundation of University of south china (grant number 2018KYY047). The Hunan Provincial Natural Science Foundation of China [2018JJ3447]; the Outstanding Youth Project of Hunan Provincial Department of Education [16B221]

References

1. T. Islamoglu, S. Goswami, Z.Y. Li, A.J. Howarth, O.K. Farha and J.T. Hupp, *Acc. Chem. Res*., 50 (2017) 805.
2. S. S. Zheng, X.R. Li, B.Y. Yan, Q. Hu, Y.X. Xu, X. Xiao, H.G. Xue and H. Pang, A*dv. Energy Mater.*, 7 (2017) 18.
3. 3.A. Kirchon, L. Feng, H.F. Drake, E.A. Joseph, H.C. Zhou, *Chem. Soc. Rev*., 47 (2018) 8611
4. Maddumapatabandi, R.P. Galhenage, B.W. Larson, O.G. Reid, S.C. Ammal, A. Heyden, M. Chandrashekhar, V. Stavila, D.A. Chen, N.B. Shustova, *J. Am. Chem. Soc*., 139 (2017) 5201.
5. I. Luz, A. Loiudice, D.T. Sun, W.L. Queen, R. Buonsanti, *Chem. Mater*., 28 (2016) 3839.
6. B.E. Conway, Electrochemical Supercapacitors, Kluwer Academic/Plenum Press, New York, 1999.
7. Y. Yan, P. Gu, S.S. Zheng, M.B. Bao, H. Pang and H. G. Xue., *J. Mater. Chem*. A., 4 (2016) 48.
8. Yang, P. Xiong, C. Zheng, H. Qiu, M. Wei, *J. Mater. Chem*. A., 2 (2014) 16640.
9. Y. Zhang, H. Feng, X. Wu, L. Wang, A. Zhang, T. Xia, H. Dong, X. Li and L. Zhang, *Int. J. Hydrogen Energy.*, 34 (2009) 4889.
10. Z.Q. Xue, Y.L. Li, Y.W. Zhang, W. Geng, B.M Jia, J. Tang, S.X. Bao, H.P. Wang, Y.Y Fan, Z.W. Wei, Z.W. Zhang, Zhuofeng Ke, G.Q. Li, C.Y. Su, *Adv. Energy Mater*., 29 (2018) 8.
11. L.Y. Zhang, D.W. Shi, T. Liu, Mietek .J, J.G. Yu, *Mater. Today*., 25 (2019) 35.
12. B.L. Chen, Z.O.B. Xue, *J. Am. Chem. Soc*., 130 (2008) 6411.
13. S.W. Gao, Y.W. Sui, F.X. Wei, J.Q. Qi, Q.K. Meng and Y.Z. He, *J. Mater. Sci*., 53 (2018) 6807.
14. H.C. Xia, J.N. Zhang, Z. Yang, S.Y. Guo, S.H. Guo, Q. Xu, *Nano-Micro Lett*., 9 (2017) 47
15. S.W. Gao, Y.W. Sui, F.X. Wei, J.Q. Qi, Q.K. Meng, Y.J. Ren and Y.Z. He, *J. Colloid Interface Sci*., 531 (2018) 23.

16. G.P. Wang, Q.T. Zhang, Z.L. Yu, M.Z. Qu, *Solid State Ionics*., 179 (2008) 263.
17. Y. Wang, S.L. Gai, C.X. Li, F. He, M.L. Zhang, Y.D. Yan, *Electrochim. Acta*., 90 (2013) 673.